Hemispheric specialization within the inferior parietal lobe across cognitive domains

Short title: Neurocognitive asymmetry in the inferior parietal cortex

Ole Numssen[1], Danilo Bzdok[2,3,#,*], Gesa Hartwigsen[1,#,*]

[1] Lise Meitner Research Group "Cognition and Plasticity", Max Planck Institute for Human Cognitive and Brain Sciences Leipzig, Germany

[2] Department of Biomedical Engineering, McConnell Brain Imaging Centre, Montreal Neurological Institute, Faculty of Medicine, McGill University, Montreal, Canada

[3] Mila - Quebec Artificial Intelligence Institute, Montreal, Canada

shared senior authorship

Main text word count: 3862
Abstract: 149

Number of Figures: 4**; Number of Tables:** 2

*Correspondence should be addressed to:

Danilo Bzdok
McConnell Brain Imaging Centre
Department of Biomedical Engineering
Montreal Neurological Institute
3801 rue University
Bureau #872D
Montréal (Québec) H3A 2B4, Canada
Phone: +1 438 524 2713
danilo.bzdok@mcgill.ca

Gesa Hartwigsen
Lise Meitner Research Group
Cognition and Plasticity
Max Planck Institute for Human
Cognitive and Brain Sciences
Stephanstrasse 1a
D-04103 Leipzig, Germany
Phone: +49 341 9940162
hartwigsen@cbs.mpg.de

Abstract

The inferior parietal lobe (IPL) is a key neural substrate underlying diverse mental processes, from basic attention to language and social cognition that define human interactions. Its putative domain-global role appears to tie into poorly understood functional differences between both hemispheres. Across attentional, semantic, and social cognitive experiments, our study explored hemispheric specialization within the IPL. The task specificity of IPL subregion activity was substantiated by distinct predictive signatures identified by multivariate pattern-learning algorithms. Moreover, the left and right IPL exerted domain-specific modulation of effective connectivity among their subregions. Task-evoked functional interactions of the anterior and posterior IPL subregions involved recruitment of distributed cortical partners. While each anterior IPL subregion was engaged in strongly lateralized coupling links, both posterior subregions showed more symmetric coupling patterns across hemispheres. Our collective results shed light on how under-appreciated lateralization effects within the IPL support some of the most distinctive human mental capacities.

Keywords: human intelligence, systems neuroscience, lateralization, human cognition, language, attention, social cognition, machine learning

Introduction

Many cognitive processes are realized by spatially distributed neural networks in the human brain. The inferior parietal lobe (IPL) is a heteromodal convergence zone of various brain networks that is central to realizing key cognitive operations across different levels of the neural processing hierarchy[1,2]. These mental operations include lower-level processes, such as spatial attention, as well as higher-level processes that are distinctly elaborate in the human species, like semantic memory and modes of social exchange.

During primate evolution, the IPL has probably undergone remarkable expansion and functional reorganization[3]. The emergence of new areas inside the human IPL has been seriously considered[4,5], while its precise correspondence to nonhuman homologues is still debated[2,6]. The evolutionary trajectory of the IPL, as part of the recent cortical expansion in humans may bear important relationships to language ability, future planning, problem solving, and other complex mental operations[2] at which humans excel.

Many cognitive capacities have been linked to neural activity in the IPL. Among these, spatial attention is crucial in an ever-changing environment that requires rapid behavioral adaptation[7]. Systematic reviews have noted a consistent trend for right-lateralization of attentional systems, with a central role of the right IPL[7]. Neurological damage of the right IPL entails a clinical condition called hemi-neglect: the failure to orient visual attention to the contralesional side[8]. In contrast to visuospatial attention, language function is widely accepted to lateralize to the (dominant) left hemisphere[9–11]. Tissue damage to the left IPL has been reported, for decades, to cause impairments of semantic processing – key to reading and other elaborate forms of language comprehension[2,6,12,13]. Semantic processing is instrumental for the human ability to contextualize and act according to the meaning of objects, events, and situations[14].

Moreover, semantic concepts are an integral component of numerous high-level cognitive operations, and are suspected to contribute to both social cognition and language from early development to adulthood[15]. Semantic processing is presumably closely intertwined with social cognition. This view receives support from previous reports on spatial overlap between both cognitive domains in the left IPL[2,6,16]. However, many human neuroimaging experiments have shown that advanced social cognitive functions, such as the capacity to infer others' thoughts, beliefs, and behavioral dispositions, tend to engage the IPL in both hemispheres[16,17].

Substantiating these earlier hints at functional specialization of left versus right IPL, both regions also differ on the structural level. Architectural heterogeneity is indicated by cytoarchitectonic borders and gyral differentiation[18,19] as well as anatomical fiber bundle connections as quantified by fiber tractography[20]. This structural scaffold has the potential to support the unique neurocognitive

properties of the left and right IPL.

Finally, the IPL harbors a major hub of the transmodal association network[21] ('default mode network') and is densely connected with other cortical key areas for various functions. This is reflected in intimate functional interactions with several other large-scale brain networks as measured by intrinsic functional connectivity[18,22,23]. Despite indications in favor of hemispheric lateralization, it remains obscure how the left and right IPL interact with distributed neural networks to realize advanced cognitive operations like social and semantic processes.

For these reasons, our study capitalized on cognitive neuroimaging experiments that tap on multiple functional domains. The combination of an arsenal of data-driven analysis techniques allowed zooming in on the functional specialization and brain-wide interaction profiles of the IPL and its segregated components. Our well-matched experimental paradigms prompted attentional reorienting, lexical decisions, and mental perspective taking – archetypical processes that exemplify the broader cognitive domains attention, semantics, and social cognition. The direct task comparison in the same sample of subjects enabled us to identify hemispheric asymmetries and involvement of common mechanisms across attentional, semantic, and social realms of human cognition. Our unique characterization of IPL function, subspecialization, and interaction patterns provides key insights into cognitive operations that underlie elaborate forms of human interaction and communication.

Results

IPL recruitment in different cognitive tasks: neural activity responses

We designed three different tasks to probe the three domains of interest. An attentional reorienting task required subjects to make spatially congruent button presses in response to visually presented cues. A lexical decision task probed visual word-pseudoword decisions and a mental perspective taking task prompted decisions on the mental beliefs of others (Fig. S1 for the experimental design and behavioral results).

We first examined neural activity responses for each task separately by contrasting each target condition (*invalid, word, false belief*) with its respective control condition (*valid, pseudoword, true belief*). In this analysis, all tasks showed increased neural activity in a widespread set of brain regions, including the IPL. Attentional reorienting led to higher neural activity in the right supramarginal gyrus, precuneus, and right superior parietal lobe, among other regions. During lexical decisions, neural activity increased in numerous left hemispheric regions, including the midcingulate cortex, angular gyrus, and superior frontal gyrus. During social cognition, distributed regions such as the supplementary motor cortex, the left inferior frontal gyrus, and the right angular gyrus were stronger activated for false beliefs (Fig. S2 and Table S1 for details).

With respect to neural activity responses in the IPL, we found strong upregulation of the right supramarginal gyrus (x, y, z = 57, -48, 24; T = 9.68) during attentional reorienting, left angular gyrus (x, y, z = -51, -72, 28; T = 8.00) during lexical decisions, and right angular gyrus (51, -60, 31; T = 5.15) during perspective taking. To summarize, standard mass-univariate analyses showed that all three tasks recruited areas within the larger IPL region in at least one hemisphere.

Functional parcellation of the IPL in two subregions

To isolate coherent structure-function mappings from neural task responses, we used data-driven clustering algorithms to separate the cytoarchitectonically constrained region of interest (ROI) in the IPL into subregions (see Methods for details). According to the applied cluster validity criteria, a two-cluster solution was indicated to be optimal in each hemisphere considering different cluster numbers. The choice of two final clusters was based on majority votes yielding 97.1% and 78.8% agreement across 25 distinct cluster validity criteria (cf. Methods) for left and right IPL, respectively (Table 1). The three-cluster solution emerged as the second best choice (left IPL: 2.8% agreement, right IPL: 21.2% agreement).

For all later analysis steps, 74 (out of 1102) voxels in the left and 84 (out of 1123) in the right IPL ROI were removed from the final solution because their cluster assignments were unstable across the random centroid initializations of the *k*-means algorithm. All discarded voxels were located at the cluster borders. The IPL parcellation procedure led to one anterior subregion (left hemisphere: L-ant, right hemisphere: R-ant) and one posterior subregion (L-post, R-post) in each hemisphere (Fig. 1B).

Hemispheric asymmetries in cluster assignment were evaluated by quantifying topographical overlap after flipping the right-left axis of the four derived IPL subregions (Fig. S3). Around two thirds of the voxels composing the IPL ROI (left: 64.98%, right: 66.31%) were spatially congruent across hemispheres. Considering these corresponding voxels contained in both left and right IPL ROI, subregion-specific across-hemisphere congruency was nearly perfect (L-ant: 88.97%; L-post: 100%; R-ant: 100%; R-post: 93.48%). The data-driven IPL parcellation into two subregions in each hemisphere served as the basis for all subsequent analyses.

Table 1. Task-derived IPL subregions

Hemisphere	Position	Label	Volume	Center of mass	Cytoarchitectonic area
Left	anterior	L-ant	11.6 cm^3	-57, -32, 30	PF, PFop, PGcm, PFt
Left	posterior	L-post	20.7 cm^3	-48, -61, 33	PGa, PGp, PFm, PF
Right	anterior	R-ant	12.9 cm^3	58, -29, 28	PF, PFop, PGcm, PFt
Right	posterior	R-post	19.8 cm^3	51, -57, 32	PGa, PGp, PFm

Note: Cytoarchitectonic assignment was performed with the SPM Anatomy Toolbox. Center of mass is given in MNI coordinates (x, y, z).

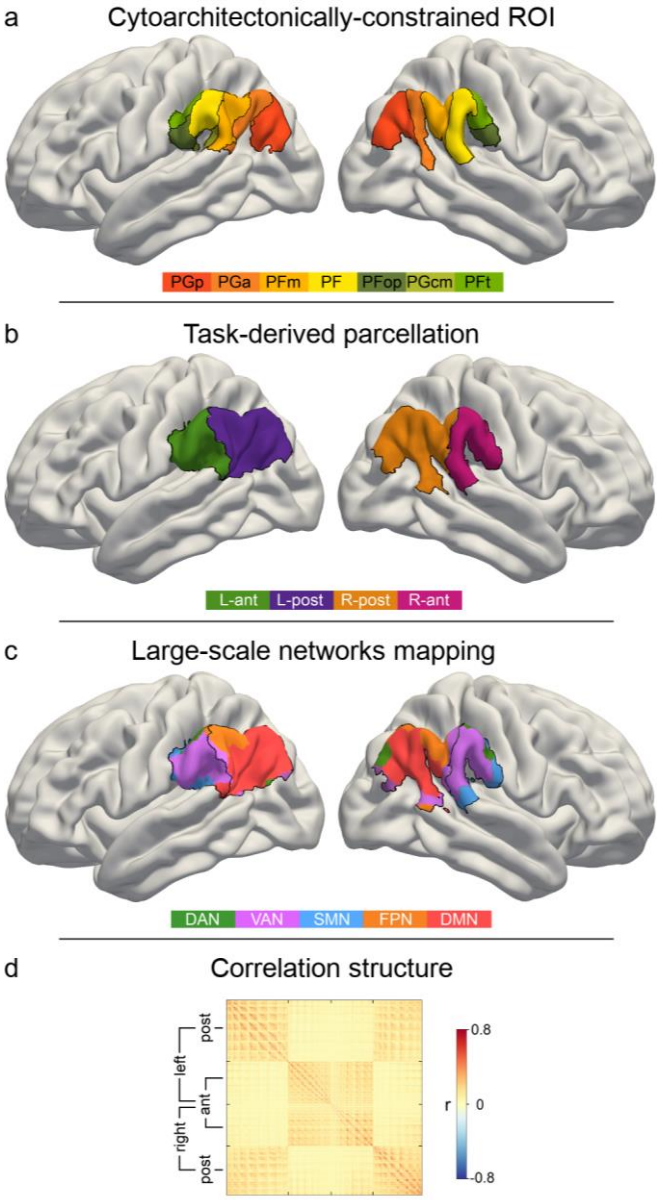

Figure 1. IPL parcellation extracted from neural activity responses across attention, semantics, and social cognition. Neural activity estimates from all three task experiments were pooled to achieve a data-driven segregation of the inferior parietal lobe, separately in each hemisphere. **(a)** Cytoarchitectonic boundaries defined the contours of our region of interest (ROI)[24]. **(b)** The derived ROI was submitted to automatic parcellation into subregions to capture neural activity profiles of the three domains in each hemisphere. L-ant: left anterior subregion. L-post: left posterior subregion. R-ant: right anterior subregion. R-post: right posterior subregion. **(c)** Mapping of large-scale brain networks[25] to the ROI. Posterior subregions are predominantly populated by the default mode network (DMN) and the anterior ventral attention network (VAN). DAN: dorsal attention network. FPN: fronto-parietal network. SMN: somatomotor network. **(d)** Similarity matrix of voxel-wise neural activity estimates of single trials, reordered according to (c). The similarity structure reproduces the parcellation results.

Task activity responses are predictive for different cognitive domains

Building on the obtained functional parcellation of the IPL into two core subregions, we investigated task-dependent hemispheric specialization of IPL function using tools from machine learning. By deploying a linear predictive pattern-learning algorithm, we solved the classification problem of assigning task-membership from single experimental trials based on the subregion-level neural activity changes. Our results indicate that neural activity response patterns from our IPL subregions alone carried relevant information that was granular enough to allow for successful task classification significantly above chance. The logistic predictive model was cross-validated in a one-versus-rest scheme to attempt classifying trial brain scans from hold-out subjects. This machine learning pipeline resulted in an overall out-of-sample classification accuracy of 52.11% (chance: 33.33%). Note that this cross-validation scheme leads to conservative accuracy estimates, as the classifier is tested on brain activity information from subjects it has not seen before.Therefore this approach provides a reliable estimate for the expected generalization in neuroimaging subjects scanned in the future[26]. Prediction accuracy reached 31.09% for the attentional reorienting task, 59.24% for the lexical decision task and 66.41% for the perspective taking task.

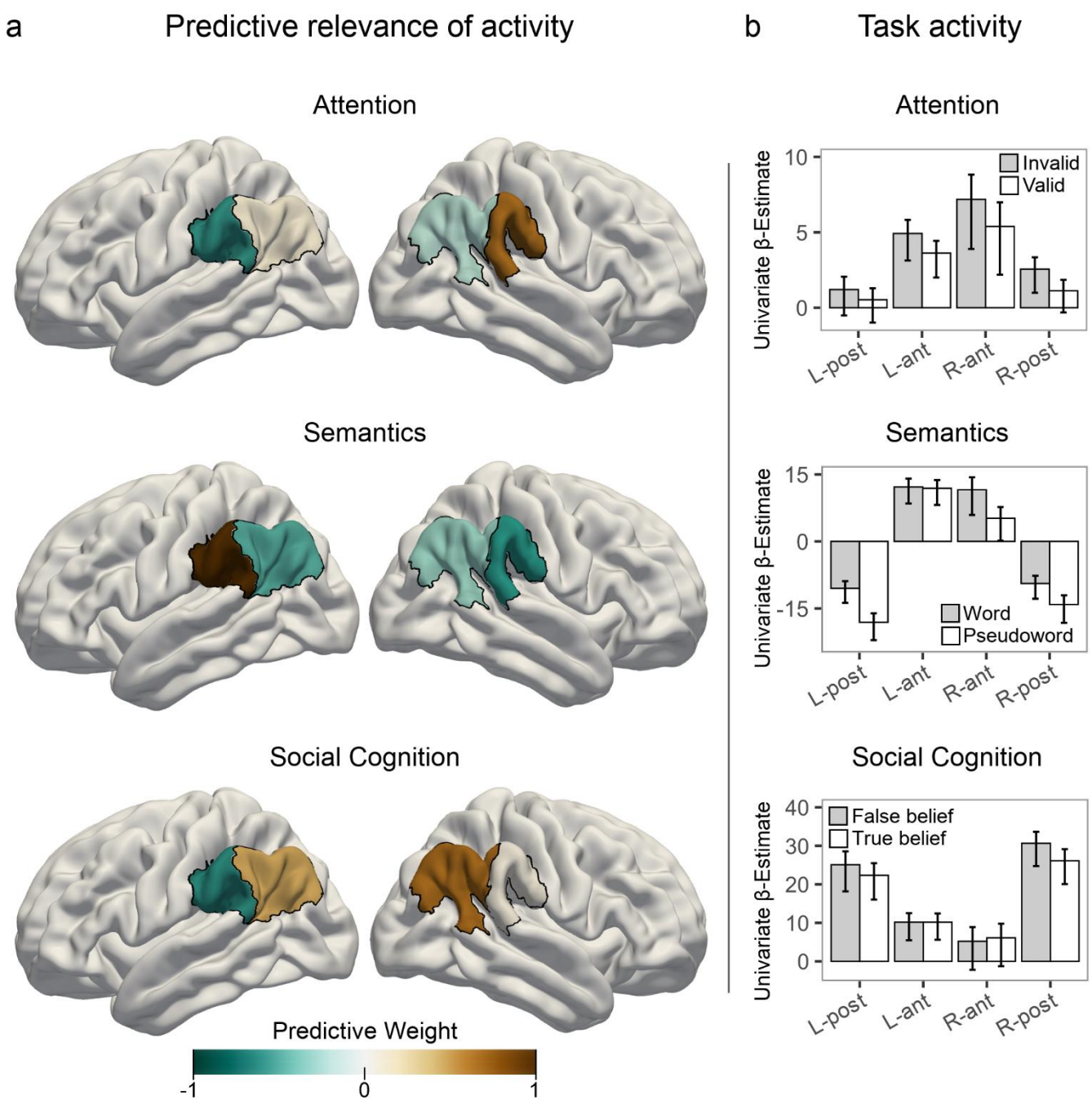

Figure 2. Task-specific predictive contributions of IPL subregions. (a) Pattern-learning algorithms extracted predictive rules from neural activity estimates aggregated in the left vs. right anterior vs. posterior IPL subregions from the three target experimental conditions for attentional reorienting (top), lexical decisions (center), and perspective taking of others' mental states (bottom). Colors show the predictive signature with relative contributions of each of the four IPL subregions in detecting the presence of the three cognitive states from neural activity responses. A more positive subregion weight (brown color) for a given task implies that neural activity from this subregion carried information that increased the probability of a specific task being represented in trial brain scans. Negative values (cold colors) denote driving the prediction decision

towards the respective other tasks. **(b)** Neural activity estimates at the center of each IPL subregion (center-of-mass). Error bars indicate 95% confidence intervals across subjects.

Relative to the other two experimental tasks, increased neural activity in the right anterior subregion and less neural activity in the left anterior subregion was associated with the attentional reorienting task when considering multivariate patterns distributed across all IPL subregions (see Fig. 2). In contrast, successful trial classification pertaining to lexical decisions was driven by neural activity increases in the left anterior subregion and neural activity decreases in the right anterior subregion, relative to the other two tasks. Finally, neural activity within both posterior subregions carried salient information that was instrumental in successfully discriminating trial brain scans recorded during perspective taking.

Task-specific network connectivity resembles task complexity

We subsequently delineated the task-dependent profiles of how IPL subregions are functionally coupled with regions outside the IPL ROI. For this purpose, we assessed functional connectivity between the four IPL subregions and other cortical brain regions. By means of non-parametric permutation testing, we tested for statistically significant coupling differences (Fig. 3 and Fig. S4). The connectivity profiles between the four IPL subregions and large-scale brain networks were significantly different between tasks. The anterior subregions showed strong degrees of hemispheric lateralization and domain specificity. In contrast, the posterior subregions showed less lateralization and a higher degree of across-network coupling.

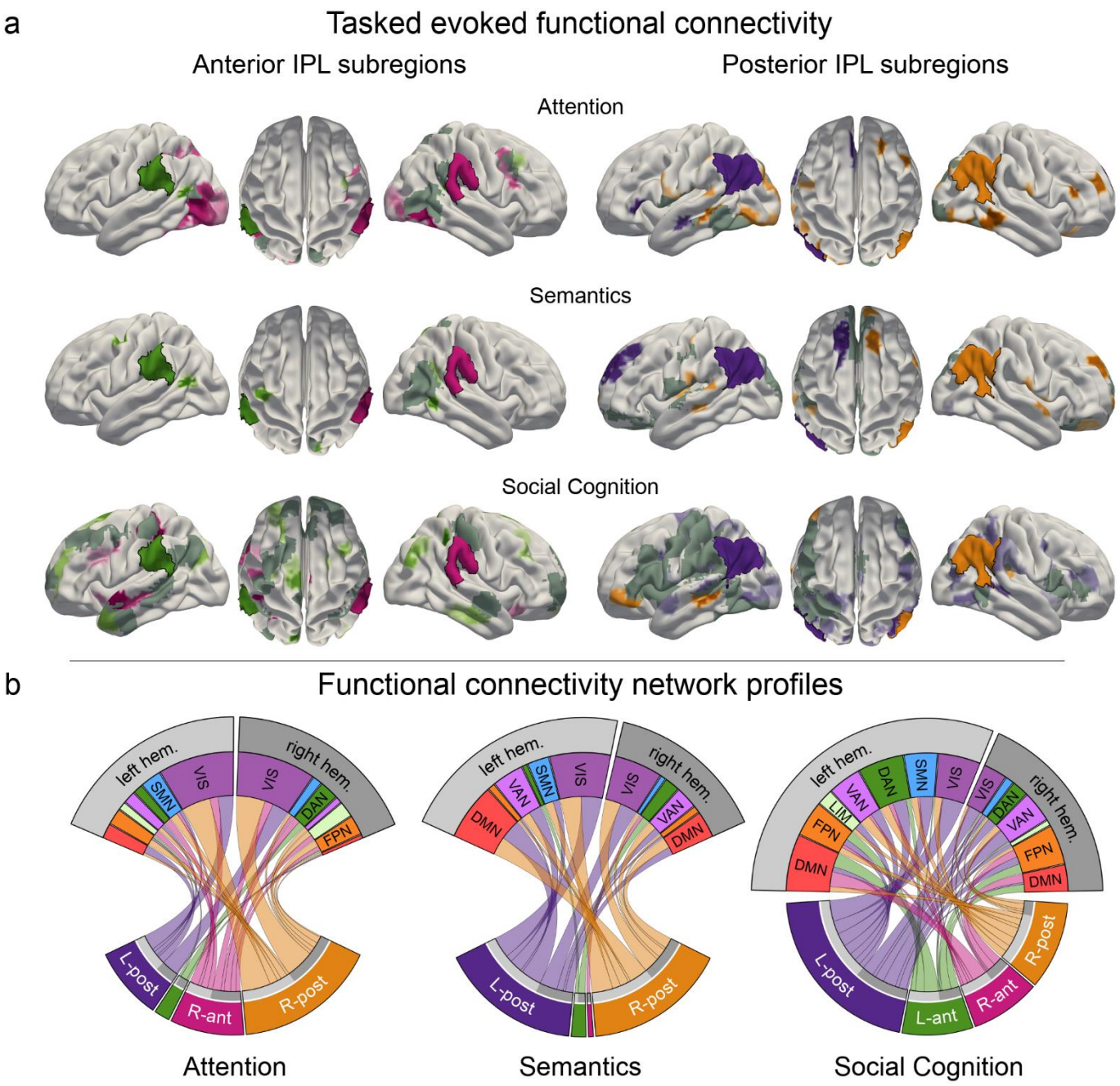

Figure 3. Task-induced shifts in cortex-wide functional connectivity. Task-dependent functional connectivity profiles of the four IPL subregions with other coupling partners compared to the respective other tasks. (**a**) Task-specific correlation between anterior (left) and posterior (right) IPL subregions and brain-wide cortical regions. All results are statistically significant at $p < 0.05$, tested against the null hypothesis of indistinguishable connectivity strength between a given IPL subregion and the rest of the brain across all three tasks. L-ant: left anterior IPL subregion; L-post: left posterior IPL subregion; R-ant: right anterior IPL subregion; R-post: right posterior IPL subregion. Dark gray: mutual connectivity target. **(b)** Task-specific connectivity profiles of the four IPL subregions with seven large-scale brain networks[25]. DAN: dorsal attention network. DMN: default mode network. FPN: fronto-parietal network. LIM: limbic network. VAN: ventral attention network. SMN: somatomotor network. VIS: visual network.

Task-specific connectivity profiles for anterior IPL subregions

During attentional reorienting, the right anterior IPL subregion was stronger involved in cortex-wide connectivity than its left-hemispheric counterpart (Fig. 4A, left column; Fig. 4D). The visual network and regions belonging to the dorsal attention network emerged as its preferred coupling partners (Fig. S4). The left anterior subregion was less engaged in cortical connectivity, and showed the strongest coupling with the dorsal attention network and the fronto-parietal control network. Compared to the other two functional domains, lexical decisions led to less cortex-wide connectivity, most strongly with left hemispheric dorsal attention network regions. In contrast, the perspective taking connectivity profiles for the left and right anterior subregions showed coupling with various networks. These IPL subregions revealed the strongest coupling patterns with left-hemispheric default mode network and bilateral fronto-parietal control network regions.

Task-specific connectivity profiles for posterior IPL subregions

During attentional reorienting, specific cortical connectivity shifts emerged for the right posterior subregion rather than the left posterior subregion of the IPL ROI (Fig. 4A, right column; Fig. 4D). Relative to the other two tasks, attentional reorienting led to significantly enhanced functional coupling with the visual network and left-hemispheric parts of the somatomotor network, as well as increased connectivity with right-hemispheric parts of the fronto-parietal control network (Fig. S4). Processing lexical decisions in turn was specifically characterized by coherent connectivity increases between the posterior IPL subregions and the bilateral visual network, the default mode network and the ventral attention network. Finally, engagement in perspective taking engendered significantly stronger functional connectivity for the left posterior subregion and extended parts of several large-scale brain networks. While the left posterior subregion showed similar connectivity strength to bilateral parts of large-scale networks, the right posterior subregion mainly interacted with contralateral parts. The posterior IPL regions showed connectivity links with multiple coupling partners, including regions belonging to the visual network, to the ventral and dorsal attention network, and to the somatomotor network.

Causal interactions between IPL subregions are task dependent

To complement our findings on the task-evoked shifts in broader cortical connectivity profiles, we used dynamic causal modeling (DCM) to identify directed task-specific connectivity modulations between IPL subregions. The DCM optimization procedure provided one Bayesian parameter average group-level model. All modulatory parameters of this optimal model exceeded zero given a 95% confidence interval. Permutation-based tests provided evidence for task-specific differences in the

emerging modulatory configurations among the IPL subregions (Fig. 4, see Table 2 for modulatory parameter estimates between subregions and Table S2 for other model parameters).

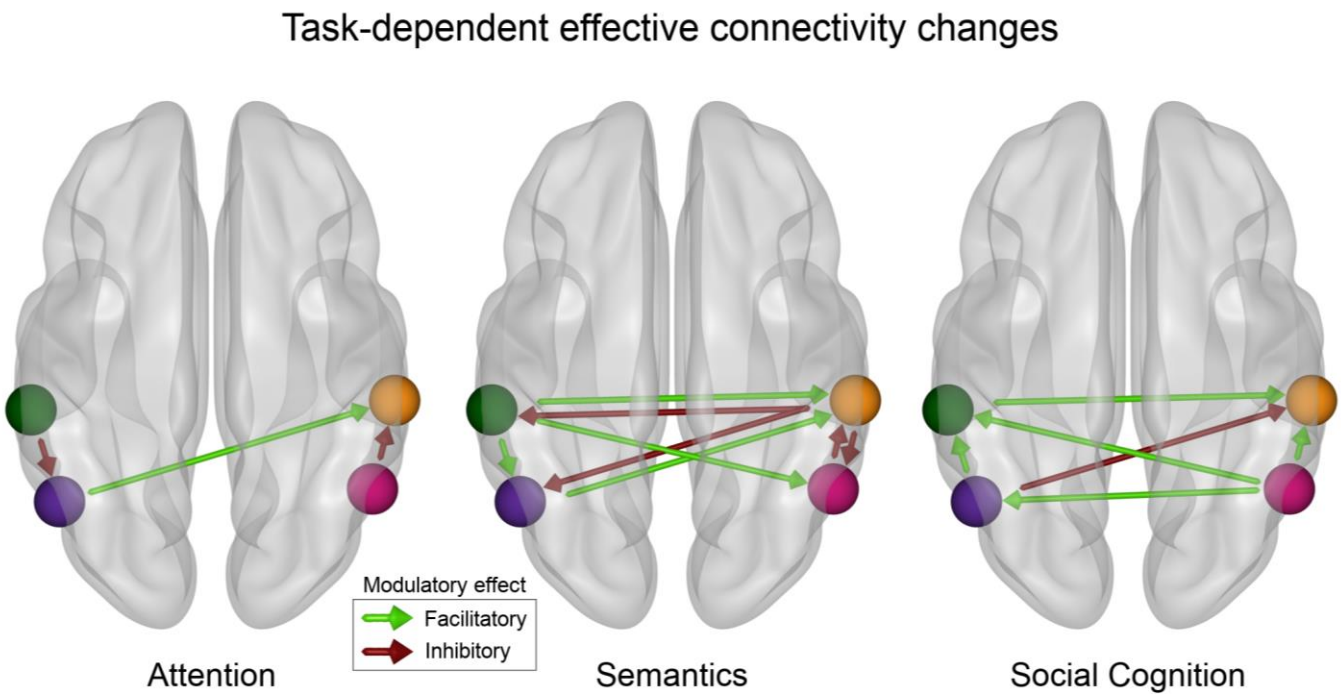

Figure 4. Tasks cause different effective connectivity modulations among IPL subregions. The modulation assessed by dynamic causal modeling (DCM) of directed connectivity among the four IPL subregions differs between attentional reorienting, lexical decisions, and perspective taking. Only significant modulatory parameters ($\alpha \leq 0.01$) are shown (based on the non-parametric permutation analysis). Attentional reorienting induces comparatively simple connectivity modulations, while both other tasks are characterized by richer changes in the modulatory influences between subregions. Lexical decisions increase facilitatory influences from the left to the right hemisphere and inhibition from the right to the left. Perspective taking causes bilateral increases in the facilitatory influence from posterior to anterior subregions. Green: DCM node in the left anterior subregion (L-ant). Violet: DCM node in the left posterior subregion (L-post). Orange: DCM node in the right anterior subregion (R-ant). Pink: DCM node in the right posterior (R-post) subregion.

Explicitly probing modulatory effects on directed connectivity within the IPL, attentional reorienting was characterized by a simple coupling configuration, with three significant modulations: An increased inhibitory influence from the left anterior to the left posterior subregion, a facilitatory drive from the left posterior to the right anterior subregion, and an inhibitory influence from the right posterior to the right anterior subregion (Fig. 4, left). The attention coupling topology was distinctively closer to the intrinsic connectivity than effective modulation patterns underlying both other domains. Both other tasks prompted more complex patterns of coupling modulations among

IPL subregions. During lexical decisions, we found strong interhemispheric modulations, both facilitatory and inhibitory, between IPL subregions. Strikingly, task-related connectivity increases from the left anterior subregion to all other subregions were facilitatory. In contrast, the right anterior subregion had an inhibitory influence on all other subregions (Fig. 4, center). Perspective taking was mainly characterized by increased facilitatory influences between IPL subregions, with the right posterior subregion exerting a facilitatory influence on all other subregions (Fig. 4, right panel). Interhemispheric interactions between subregions were also mainly facilitatory during perspective taking (Fig. 4, left).

To summarize, the three cognitive domains of interest were characterized by fundamentally different motifs of effective connectivity modulations among IPL subregions. A core observation relies on a simple directed connectivity profile for attentional reorienting and more complex directed connectivity interactions between IPL subregions for both higher-level tasks.

Table 2: Task-specific effective connectivity modulation

Source subregion		Target subregion	Modulation strength	p-value
Attention				
L-ant	→	R-post	-1.93	0.0017
L-post	→	R-ant	3.01	0.0033
R-post	→	R-ant	-1.50	0.0007
Semantics				
L-ant	→	L-post	1.08	0.0012
L-ant	→	R-ant	0.97	<0.0001
L-ant	→	R-post	1.27	0.0026
L-post	→	R-ant	1.26	<0.0001
R-ant	→	L-ant	-1.49	0.0031
R-ant	→	L-post	-2.45	0.0001
R-ant	→	R-post	-3.24	<0.0001
R-post	→	R-ant	-0.22	<0.0001
Social Cognition				
L-ant	→	R-ant	0.30	0.0078
L-post	→	L-ant	1.23	<0.0001
L-post	→	R-ant	-0.57	0.0013
R-post	→	L-ant	1.76	<0.0001
R-post	→	L-post	1.43	<0.0001
R-post	→	R-ant	2.13	<0.0001

Significant modulatory parameters ('B-matrix', $\alpha \leq 0.01$) between subregions. Based on a random effects permutation test for the null hypothesis 'no parameter difference between tasks'. The strength is given as posterior expectation from the optimum Bayesian parameter average model.

Discussion

The inferior parietal lobe is a foremost convergence zone of diverse mental capacities, several of which are potentially most developed in the human species. However, it remains open to question how some of the most basic and some of the most advanced cognitive processes converge and diverge in the IPL to realize human communication and interaction. To systematically address this unresolved issue, we carried out a multi-method investigation that makes the hemispheric specialization within the IPL apparent across attention, semantics, and social cognition experiments. Pooling insight from predictive, causal, and functional coupling analyses revealed a functional triple dissociation between the probed cognitive domains in the IPL at subregion-resolution. To foreshadow an overarching theme emerging from our findings, right-hemispheric specialization was prominent in attentional reorienting and left-hemispheric specialization in semantic processing. In contrast, both left and right IPL were robustly engaged when subjects adopted the mental perspectives of others.

The degree of functional specialization of the IPL has been contemplated before[2]. Yet, only in recent years direct comparison of task experiments from different cognitive neuroscience domains, conventionally studied in isolation, has enjoyed increasing attention[16,27–29]. Our present study invigorates these beginning endeavors to transcend cognitive fields that are typically studied independently by separate research communities. We strive towards such cross-pollination across disparate literature streams.

To pursue this goal, we show that domain-specific functional signatures became apparent within the IPL when interrogating neural activity responses to tasks, derived predictive principles, as well as modulations of directed connectivity among IPL subregions and their functional coupling profiles with distributed brain regions. It is a key advantage that our findings were based on carefully controlled experimental paradigms that were administered to the same subject sample. Consequently, our study offers critical new elements of synthesis that pave the way for a more holistic perspective of IPL specialization and a more complete understanding of its role in hemispheric asymmetry.

First, the *right* IPL showed strong engagement in attentional processes in our study. Previous work has demonstrated a causal relation between tissue damage to the right IPL and left spatial neglect[30]. Such neurological patients routinely fail to process cues in their contralesional visual field. Additionally, transient virtual lesions of the right, but not left IPL in the intact human brain were reported to cause performance declines during attentional reorienting[31]. Our findings corroborate and detail this previous research by carefully locating attentional processing and accompanying functional coupling shifts preferentially to the anterior subregion of the right IPL, compared to semantics and social cognition. Moreover, neural activity in the right anterior IPL subregion contained information that enabled successfully discriminating attentional reorienting from semantics and social cognition

in our predictive modeling analyses. The new insights on right-hemispheric lateralization of attentional reorienting in the IPL were further refined by unique and simple effective connectivity modulations between IPL subregions. Additionally, our analyses of global functional coupling patterns revealed that the right anterior IPL subregion stands out by its connections to bilateral fronto-parietal and visual-sensory networks. Together, these findings speak to a specialized neuronal infrastructure harbored within the right anterior IPL, which is especially tuned to processing demands of attentional reorienting.

Second, our results isolate strong engagement of the anterior subregion of the *left* IPL for semantic processing. Deficits in various facets of semantic processes, such as in Wernicke's aphasia[32], have received evidence to be closely linked to left temporo-parietal damage[33] among other regions of the language network. Consistently, transient virtual lesions of the left IPL in healthy subjects were reported to entail diminished performance in different semantic tasks[34,35]. Our findings from mapping neural responses during experimental tasks and identifying most predictive subregions reliably situated semantic processing in the left *anterior* IPL subregion. In addition, our effective connectivity analyses revealed a motif of rich modulatory influences among IPL subregions during semantic processing compared to our other two tasks. Specifically, we found increased task-induced facilitatory coupling from the left to the right IPL, with the anterior IPL increasing its facilitatory influence on all other subregions during semantic processing. The strong facilitatory modulation exerted from the left to the right IPL was complemented by increased inhibition in the influence of the right on the left IPL and between right-hemispheric IPL subregions, potentially reflecting cognitive control processes (e.g. inhibition of alternative responses). This constellation of task-induced connectivity modulations is consistent with an interpretation of fine-grained interactions between left and right IPL subregions, rather than an exclusive role of the dominant left hemisphere in language processing (see also [12,36,37]).

Third, adding to the right and left anterior IPL's preferential involvement in attentional and semantic processing, respectively, our perspective taking task highlighted the posterior subregion of the IPL in *both* hemispheres as key regions for social cognition. This last piece of the functional triple dissociation in the IPL received support from our multivariate predictive algorithm approach, and was further annotated by our effective connectivity examination. When subjects were concerned with inferring others' mental states, both posterior IPL subregions increased their facilitatory influence on the bilateral anterior IPL subregions. The overall task-specific connectivity configuration derived for our social cognition task was predominantly facilitatory, pointing towards tight intra- and interhemispheric interactions during mental perspective taking. A posterior-to-anterior transition of the neurocognitive processes subserved by the IPL has been proposed in previous research[16,38]. These authors identified the posterior IPL as relatively higher associative and more domain-general

processing hub, compared to the anterior IPL subregions. More broadly, the observed bilateral IPL engagement in widely employed social cognition experiments carefully reconciles previous virtual lesion evidence on the functional relevance of the overall right[39] or left[40] IPL region for social cognitive functions.

Our compilation of findings provides a multi-perspective answer to the functional subspecialization of the IPL that spans lower and higher cognitive processes. Previous studies have hinted at or considered the possibility of several specialized subregions in the IPL[1,16,29,41]. While some authors have advocated a monolithic functional role of the IPL, others advertised the possibility of functionally distinct neuronal populations in the IPL, which may be challenging to disentangle using conventional contrast analysis in neuroimaging. To the best of our knowledge, we are first to conduct a within-subject study across such a diversity of cognitive domains. Thereby, we demonstrate that cognitive processing in the IPL can probably not be accounted for by a simplistic account of functional specialization.

Rather, our complementary set of findings indicate that task-specific effective connectivity modulations within and from different IPL subregions uniquely characterize each of the probed cognitive domains. For low-level processes, here exemplified by attentional reorienting, task-specific coupling adjustment implicated a reduced set of coupling partners. In contrast, for more complex tasks, as exemplified by lexical decision and perspective taking, we found evidence for more elaborate coupling motifs, including dense intra- and inter-hemispheric facilitation and inhibition. Notably, there is a scarcity of existing studies directly devoted to investigating the left versus right IPL in several different psychological tasks (see [42,43] for exceptions). The few existing studies committed to the effective connectivity of the IPL mainly focused on task-related connectivity changes between an IPL subregion and other areas of a specialized network for a single cognitive domain, typically in one hemisphere only[34,44–46]. As such, our results usher towards a broader perspective. We complement the identification of intra- and inter-hemispheric IPL coupling patterns with strong domain-specific coupling profiles from IPL subregions to disparate cortical partners from large-scale brain networks.

Task-induced shifts in functional connectivity revealed key distinctions in interactions with major brain networks. Functional coupling profiles varied significantly between the three experimental tasks. Across domains, coupling partners were recruited from various large-scale brain networks. Our observation reinforces the notion of the IPL interfacing multiple neural systems and different levels of neurocognitive abstraction[2,29,47].

Moreover, we show that the task-specific coupling profiles between IPL subregions and a variety of cortical partners are anchored in the functional compartments uncovered in the IPL. The

wider functional connectivity profiles for the anterior and posterior subregions further elucidate their features of underlying neural processing. As a tendency, functional connectivity profiles for the left and right *posterior* subregions were similar within each task. Yet, global connectivity profiles varied between the left and right *anterior* subregions of the IPL. The hemisphere-specific functional coupling for the anterior IPL subregions is broadly consistent with the common reports of right-hemispheric specialization of attentional reorienting processes[31,48] and left-hemispheric specialization for semantic processes[12,13,21]. The rich connectivity profiles of the left and right posterior IPL subregions support the notion of bilateral IPL relevance for social cognitive processes, consolidating previous findings[16,29,49].

Specifically, during attentional processing, the dedicated coupling partners of the *right anterior* IPL subregion included regions of the visual cortex and the dorsal attention network. During semantic processing, the *left anterior* subregion enhanced coupling with regions of the default mode and ventral attention network. Ultimately, during social cognition processing, the *left and right posterior* IPL subregions preferably coupled with the default mode network. The observed task-specific functional coupling of the posterior subregions with major brain networks was largely symmetric across both hemispheres. To summarize our integrated experimental and computational study, we provide evidence for a functional triple dissociation in the human IPL, with task-specific functional specialization in distinct IPL subregions. This emerging view is supported by information carried in precise multivariate predictive signatures. Zooming into task-specific coupling motifs among IPL subregions, our effective connectivity analyses revealed that attentional reorienting mediated simpler coupling modulations, while semantic and social cognition were realized by more complex inter-hemispheric influences. Delineating task-evoked shifts in functional coupling patterns, in turn, uncovered that the *posterior* IPL subregions were linked to bilateral, symmetric recruitment of distributed cortical coupling partners, reminiscent of the default mode network. Conversely, the *anterior* IPL subregions were engaged in flexible and hemisphere-specific coupling patterns with brain-wide cortical partners. Together, our results shed new light on how currently under-appreciated lateralization profiles within the left and right IPL support some of the most distinctive mental capacities in humans.

Methods

Subject sample

Twenty-two healthy, native German speakers (11 female, mean age 37.9 ±3.28 years) participated in this neuroimaging investigation. All subjects had normal or corrected-to-normal vision and no contraindications against magnetic resonance imaging (MRI). Subjects were recruited from the inhouse database at the Max Planck Institute for Human Cognitive and Brain Sciences. Written informed consent was obtained from all subjects before the experiment. All subjects were right-handed (laterality index[50] ≥80%). The study was performed according to the guidelines of the Declaration of Helsinki and approved by the Ethics Committee of the Medical Faculty of the University of Leipzig, Germany.

Experimental design

The functional MRI (fMRI) investigation (see Fig. S1A) consisted of three sessions that were performed on separate days, scheduled at least seven days apart from each other. Each fMRI session was divided into four runs. In all runs, each of the three tasks (i.e., attentional reorienting, lexical decisions, and perspective taking, see below for details) was administered consecutively in a task block. Within task blocks, trials were presented in an event-related fashion. Each run consisted of 40 attentional reorienting trials (8 *invalid*, 30 *valid*, 2 *catch* trials), 40 lexical decision trials (20 *word* and 20 *pseudoword* trials), and 6 perspective taking trials (3 *false belief* and 3 *true belief* trials). Each stimulus for the lexical decision and social cognition task was only shown once per subject, while the attentional reorienting task relied on simple geometric cues that were presented repeatedly. At the beginning of each task block, instructions were presented. Task order was pseudo-randomized. Trial order and timing were defined by a genetic algorithm for optimizing detection power, using an adapted version of Neurodesign v0.2.1[51]. All experimental tasks were administered with Presentation Software (v20.1; Neurobehavioral Systems, Albany, USA). Prior to the first fMRI session, subjects underwent a short training for all three tasks outside the MRI scanner. Training stimuli were not included in the main experiment.

Tasks

For each probed cognitive domain, we elected a well-established task. Task presentation and response selection were carefully matched across tasks, including visual stimuli and binary choices for all tasks. All three tasks conformed to the principle of using a single target condition and a single control condition to isolate the neural activity of the particular cognitive function. In all three tasks, subjects responded to a binary choice after each trial via button press. Button assignments were randomized across subjects and kept identical across sessions. Subjects were instructed to respond as fast and

accurately as possible. Example trials for each of the different tasks and conditions are available in Fig. S1.

Attention

We used a Posner-like attentional reorienting task, as described previously[31]. Each trial started with the presentation of two rectangular, empty boxes (size 2.6° of visual angle, center distance 8.3°, positioned horizontally) and a fixation cross at the center of the screen (Fig. S1B). After an average duration of 3.2 s (*SD* = 1.41 s, minimum interstimulus interval = 2 s), the fixation cross was replaced with an arrow pointing either to the right or the left for 250 ms or 350 ms (the 'cue'). Subsequently, a target asterisk was presented in one of the rectangles. In 75% of the trials, the target location was congruent with the direction of the arrow (*valid* condition). In 20% of the trials, the target was presented on the (unexpected) opposite side (*invalid* condition). In 5% of the trials, no asterisk was shown (*catch* condition) and no response was probed to ensure constant attention. Subjects were asked to indicate the location of the target with a button press. Note that the *invalid* condition was intended to recruit attentional reorienting processes. Instead, the *valid* condition served as the matched control condition.

Semantics

We administered a lexical decision task that contrasts words and pseudowords as a prototypical example of semantic processing[52,53]. 240 concrete German nouns were selected from the SUBTLEX-DE database[54]. Inclusion criteria were i) two syllables; ii) frequency per million > 1; iii) concreteness ratings < 4; and iv) arousal ratings < 6, according to the LANG rating (note that smaller values correspond to a higher concreteness[55]). All word stimuli denoted countable entities and were non-ambiguous. A pseudoword was created for each word with Wuggy v0.2.2b2[56] to assure phonotactic validity without semantic content. Pseudowords matched their word counterparts in length, syllable structure, and transition frequencies between subsyllabic elements. Each trial started with the presentation of a fixation cross for at least 2 s (*M* = 3.8 s, *SD* = 1.7). Thereafter, a word (target condition) or pseudoword (control condition) was shown for 1 s. Subjects were instructed to indicate whether the stimulus represented a word or pseudoword via button press (Fig. S1C).

Social cognition

For the perspective taking task, we employed an adapted version of the Sally-Anne paradigm[57,58], which is known to prompt reasoning about the mental state of others[59]. In total, 72 three-picture comics were presented, with 2 s presentation time per stimulus. Between trials, a fixation cross was shown for at least 2 s (*M* = 3.8 s, *SD* = 1.7 s). In all trials, character A puts an object into a container-like object (picture 1). Then character B passes the object on to another container. Character A either observes this action (*true belief* condition) or not (*false belief* condition) (picture 2) and then searches

in either the correct or in the wrong location (picture 3). Subjects were instructed to indicate whether the search location was congruent or incongruent with character A's knowledge about the object position via button press (Fig. S1D). A correct response in the *false belief* condition required the subject to infer the mental state of character A from the comic narrative. In contrast, for the control condition (*true belief)*, a correct response did not depend on perspective taking and could be accomplished by relying on the physical reality shown to the subjects.

Classical statistical analysis

At the single-subject level, two design matrices were specified and general linear models (GLMs) were computed using SPM12 (Wellcome Department of Imaging Neuroscience, London, UK). GLM_{cond} was designed with one regressor per condition in accordance with the standard mass-univariate analysis. The second set of GLMs (GLM_{trial}) was purpose-designed for multivariate and task-related functional connectivity analyses with one regressor per trial to gain access to trial-wise neural activity estimates[60]. See SI for details on the GLM specifications and contrast definitions. Details on MRI parameters and preprocessing are also provided in the supplementary information.

Subregion identification in the IPL

The topographical outline for the left and right IPL ROI was guided by an established and freely available histological atlas. Seven cytoarchitectonic maps cover the human IPL in each hemisphere[18] according to the widely used JuBrain probabilistic cytoarchitectonic atlas[61]. These anatomical definitions of microstructurally defined areas known to exist in the IPL comprised one rostral (PGp) and one caudal (PGa) region in the angular gyrus, and five regions of the supramarginal gyrus (PFm, PF, PFop, PGcm, PFt), as provided by the SPM 12 Anatomy Toolbox v2.2b[62]. The outer boundary of the conglomerate of these cytoarchitectonic areas was taken as contours of our ROI in the IPL, separately in the left and right hemisphere. Both of our ensuing ROI definitions occupied similar cortical volume: 1102 voxels in the left and 1123 voxels in the right (Fig. 1A) hemisphere.

We used tools from machine learning to explore coherent solutions to IPL segregation in the context of our experimental tasks. A *k*-means clustering[63–65] was applied at the voxel level with 1,000 random centroid initializations[66] based on the estimates from the "target condition > rest" contrast of the GLM_{cond} in the IPL ROIs. The unsupervised clustering algorithm was applied on pooled information across subjects and separately for each hemisphere. To explore an optimal number of clusters, hemisphere by hemisphere, our choice was anchored in the majority vote taken across 25 distinct cluster validity metrics that were computed for candidate solutions with 2 to 7 clusters using NBClust v3.0[67]. Each cluster quality metric provided a ranking of candidate cluster numbers based on a different notion of goodness-of-fit of the candidate solutions. The majority vote of these different ranking criteria provided a principled, data-driven rationale for the final cluster number that we

endorsed in our study, in each hemisphere[64]. To ensure robust voxel-to-cluster assignments, all solutions from the 1,000 algorithms initializations that resulted in the winning cluster number were merged into one final solution. Specifically, the final assignments of voxel-to-cluster responsibilities were based on agreement across the random algorithm initializations. Voxels with varying cluster allocations across the initializations were excluded from the final cluster solution (cf. results section).

Task-predictive information of the IPL subregions

After establishing functionally defined subregions in our IPL ROIs, we directed attention to the information content available at subregion granularity. For this purpose, we carried out a one-versus-rest scheme in combination with a sigmoid-loss (logistic) linear predictive algorithm to automatically detect the task membership of single experimental trials directly from subregion-wise averaged neural activity signals. Model parameter estimation and model evaluation of predictive success were performed conjointly for the three target conditions (*invalid*, *word*, *false belief*). This modeling strategy naturally yielded a set of predictive weights for all subregions for each task. Appropriately balanced numbers of trials were ensured for all conditions by sub-sampling to the minimum number of trials per subject and fMRI run. We exclusively considered task trials and brain scans with correct responses. Signal deconfounding removed variation that could be explained by session number, session time, subject identify or run time. A run-wise variable standardization was applied, before model estimation, by de-meaning to zero and unit-variance scaling to one. The generalization performance of the prediction accuracy was estimated via leave-one-subject-out cross-validation. Brain scans from a given subject therefore appeared only either among the brain scan information (training data) used for model estimation or the brain scan information (testing data) used to put the already-fitted predictive model to the test. The parameters of the predictive algorithm were averaged across all cross-validation folds to guard against noise and obtain a single final predictive model solution for inspection and visualization[1]. The pattern-classification pipelines were realized in the Python data science ecosystem, using especially nilearn v0.6.2[68] and scikit-learn v0.21.2[69]. Overall, the set of multivariate predictive analyses thus aimed at revealing task-distinctive information available at subregion-level signals in our IPL ROIs.

Task-evoked functional connectivity shifts

We then quantitatively characterized the task-induced changes in distributed functional coupling profiles as anchored in each of the IPL subregions. Analogous to the multivariate pattern recognition approach (cf. last paragraph), this cortex-wide analysis was performed across the three distinct task contexts. We drew on the commonly used Schaefer-Yeo atlas[70] (v0.15.3) with 400 parcels to parse the distributed neural activity estimates (GLM_{trial}) of the three target conditions (*invalid*, *word*, *false belief*). Consistent with the other analysis approaches, we discarded any trials with incorrect subject

responses. Neural activity estimates were summarized by averaging across all voxels belonging to a given IPL subregion. For each experimental target condition, Pearson's correlation coefficients were computed between a given IPL subregion and each of the Schaefer-Yeo parcels. To rigorously assess whether connectivity links between a specific IPL subregion and cortical parcel were reliably weaker or stronger in one task relative to the other two, a pooled permutation-based baseline was computed across all three task conditions. Task-specific functional coupling shifts were determined by statistical significance testing based on a non-parametric permutation procedure using an empirical null-hypothesis distribution[26,71]. The data-derived null model reflected the constellation of neural activity coupling strengths between a given subregion and other cortical regions that would be expected if task A induced similar patterns of brain connectivity, compared to the respective other tasks B and C. Following this fully data-driven analysis tactic, for each of the three tasks, the analysis directly provided brain maps of task-dependent functional connectivity profiles for the IPL subregions.

Task-specific effective connectivity modulation

After delineating (undirected) functional connectivity of IPL subregions with brain-wide cortical regions, we explicitly examined task-dependent causal interactions within the IPL. To achieve this goal, we analyzed the effective connectivity among the four IPL subregions by means of DCM[72]. Since this approach centered on the directed interaction among the IPL subregions themselves, this analysis selectively included these four compartments. Effective connectivity was estimated with DCM 12.5[72] implemented in SPM 12. We defined and deployed subject-wise DCMs with one target node per subregion. Subject-specific node centers per subregion were based on the peak activity across all three tasks. We ensured similar contribution of all tasks by task-wise normalization of neural activity estimates to define the subject-wise DCM nodes. The first eigenvariate from the timeseries of voxels in an 8mm sphere around this target was extracted[73]. We exclusively included data from voxels within the upper quartile of estimated neural activity to ensure functional relevance[74] and assured that all voxels fell into the respective IPL subregion. A fully connected DCM (full model) estimated all possible connections among the four IPL subregions (including self-connections) and directions of modulatory influences. The trial onsets of the three target conditions were modeled as direct inputs to the nodes and as modulatory inputs to the inter-regional connections. Neural activity stemming from incorrect trials and control conditions was regressed out[73].

After model estimation, subject-wise full models were optimized for the intrinsic connections (*A* matrix) and modulatory inputs (*B* matrix) at the group level using the Bayesian model selection procedure[75]. We decided against optimization of the input parameters (*C* matrix), as we selectively modeled nodes in high-order association cortex. As such, there was no obvious scientific hypothesis regarding the input to the system. The optimized, reduced model represented fixed-effects at the

group level[76,77]. As a second-level random-effects analysis, we conducted a non-parametric permutation test on subject-wise parameters of the optimal reduced model. This layer of analysis identified those model parameters that varied significantly between tasks. Specifically, for each task, the parameter differences of the remaining two tasks were randomly shuffled 10,000 times to obtain and test against an empirical distribution for the null hypothesis (i.e., no differences between task-dependent effective connectivity). Statistical significance was determined based on the absolute parameter difference higher than 99.9% of the baseline difference, corresponding to $\alpha \leq 0.01$.

Brain results were rendered by means of Paraview v5.7.0[78], circlelize v0.4.8[79] and BrainNet Viewer v1.7[80]. To this end, results were transformed from MNI space (ICBM 152 linear[81]) to the surface-based FreeSurfer fsaverage[82] coordinate system via the nonlinear mapping Registration Fusion approach v0.6.5[83].

Acknowledgements

This work was supported by the German Research Foundation (BZ2/4-1, BZ2/3-1, and BZ2/2-1 to DB and HA 6314/3-1 and HA 6314/4-1 to GH), the NVIDIA Corporation (donation of a Titan Xp graphics card to GH), and National Institutes of Health (NIH grant R01AG068563A to DB). DB was further supported by the Healthy Brains Healthy Lives initiative (Canada First Research Excellence fund), by the CIFAR Artificial Intelligence Chairs program (Canada Institute for Advanced Research), and by Google (Research Award). GH was further supported by the Lise-Meitner excellence program of the Max Planck Society.

Author Contributions

DB and GH conceptualized the study, DB, GH, and ON designed the experiment. GH and ON performed the experiments. DB, GH, and ON analyzed the data, interpreted the results and wrote the manuscript.

Competing Interests statement

The authors declare that no competing interests exist.

Data Availability

Data is made available from the authors upon reasonable request. Restrictions might apply due to the General Data Protection Regulation (EU).

Code availability

All self-written code that was used to prepare the experiment and for analyzing the data is made available: http:// gitlab.gwdg.de/IPLplasticity/FuncSeg

References

1. Kernbach, J. M. *et al.* Subspecialization within default mode nodes characterized in 10,000 UK Biobank participants. *Proc. Natl. Acad. Sci. U.S.A.* **115**, 12295–12300 (2018).
2. Seghier, M. L. The angular gyrus: multiple functions and multiple subdivisions. *Neuroscientist* **19**, 43–61 (2013).
3. Van Essen, D. C. & Dierker, D. L. Surface-based and probabilistic atlases of primate cerebral cortex. *Neuron* **56**, 209–225 (2007).
4. Orban, G. A., Van Essen, D. & Vanduffel, W. Comparative mapping of higher visual areas in monkeys and humans. *Trends Cogn. Sci.* **8**, 315–324 (2004).
5. Mars, R. B., Sallet, J., Neubert, F.-X. & Rushworth, M. F. S. Connectivity profiles reveal the relationship between brain areas for social cognition in human and monkey temporoparietal cortex. *Proc. Natl. Acad. Sci. U. S. A.* **110**, 10806–10811 (2013).
6. Mars, R. B. *et al.* Diffusion-weighted imaging tractography-based parcellation of the human parietal cortex and comparison with human and macaque resting-state functional connectivity. *J. Neurosci.* **31**, 4087–4100 (2011).
7. Corbetta, M., Patel, G. & Shulman, G. L. The reorienting system of the human brain: from environment to theory of mind. *Neuron* **58**, 306–324 (2008).
8. Morrow, L. A. & Ratcliff, G. The disengagement of covert attention and the neglect syndrome. *Psychobiology* **16**, 261–269 (1998).
9. Friederici, A. D. Evolution of the neural language network. *Psychon Bull. Rev.* **24**, 41–47 (2017).
10. Hickok, G. & Poeppel, D. The cortical organization of speech processing. *Nat. Rev. Neurosci.* **8**, 393–402 (2007).
11. Cai, Q., Van der Haegen, L. & Brysbaert, M. Complementary hemispheric specialization for language production and visuospatial attention. *Proc. Natl. Acad. Sci. U.S.A.* **110**, E322–30 (2013).

12. Binder, J. R., Desai, R. H., Graves, W. W. & Conant, L. L. Where Is the semantic system? A critical review and meta-analysis of 120 functional neuroimaging studies. *Cereb. Cortex* **19**, 2767–2796 (2009).

13. Hartwigsen, G. *et al.* Dissociating parieto-frontal networks for phonological and semantic word decisions: A condition-and-perturb TMS study. *Cereb. Cortex* **26**, 2590–2601 (2016).

14. Lambon Ralph, M. A. & Patterson, K. Generalization and differentiation in semantic memory: insights from semantic dementia. *Ann. N. Y. Acad. Sci.* **1124**, 61–76 (2008).

15. Binder, J. R. & Desai, R. H. The neurobiology of semantic memory. *Trends Cog. Sci.* **15**, 527–536 (2011).

16. Bzdok, D. *et al.* Left inferior parietal lobe engagement in social cognition and language. *Neurosci. Biobehav. Rev.* **68**, 319–334 (2016).

17. Schurz, M., Radua, J., Aichhorn, M., Richlan, F. & Perner, J. Fractionating theory of mind: a meta-analysis of functional brain imaging studies. *Neurosci. Biobehav. Rev.* **42**, 9–34 (2014).

18. Caspers, S. *et al.* The human inferior parietal cortex: cytoarchitectonic parcellation and interindividual variability. *Neuroimage* **33**, 430–448 (2006).

19. Caspers, S. *et al.* The human inferior parietal lobule in stereotaxic space. *Brain Struct. Funct.* **212**, 481–495 (2008).

20. Caspers, S. *et al.* Probabilistic fibre tract analysis of cytoarchitectonically defined human inferior parietal lobule areas reveals similarities to macaques. *Neuroimage* **58**, 362–380 (2011).

21. Braga, R. M., DiNicola, L. M. & Buckner, R. L. Situating the left-lateralized language network in the broader organization of multiple specialized large-scale distributed networks. *bioRxiv* (2019) doi:10.1101/2019.12.11.873174.

22. Buckner, R. L. & DiNicola, L. M. The brain's default network: updated anatomy, physiology and evolving insights. *Nat. Rev. Neurosci.* **20**, 593–608 (2019).

23. Raichle, M. E. *et al.* A default mode of brain function. *Proc. Natl. Acad. Sci. U.S.A.* **98**, 676–682 (2001).

24. Zilles, K. & Amunts, K. Centenary of Brodmann's map — conception and fate. *Nat. Rev. Neurosci.* **11**, 139–145 (2010).

25. Yeo, B. T. T. *et al.* The organization of the human cerebral cortex estimated by intrinsic functional connectivity. *J. Neurophysiol.* **106**, 1125–1165 (2011).

26. Bzdok, D. & Yeo, B. T. T. Inference in the age of big data: Future perspectives on neuroscience. *Neuroimage* **155**, 549–564 (2017).

27. Humphreys, G. F. & Lambon Ralph, M. A. Fusion and fission of cognitive functions in the human parietal cortex. *Cereb. Cortex* **25**, 3547–3560 (2015).

28. Igelström, K. M., Webb, T. W., Kelly, Y. T. & Graziano, M. S. A. Topographical organization of attentional, social, and memory processes in the human temporoparietal cortex. *eNeuro* **3**, 1–12 (2016).

29. Bzdok, D. *et al.* Characterization of the temporo-parietal junction by combining data-driven parcellation, complementary connectivity analyses, and functional decoding. *Neuroimage* **81**, 381–392 (2013).

30. Thiebaut de Schotten, M. *et al.* Damage to white matter pathways in subacute and chronic spatial neglect: a group study and 2 single-case studies with complete virtual 'in vivo' tractography dissection. *Cereb. Cortex* **24**, 691–706 (2014).

31. Rushworth, M. F., Ellison, A. & Walsh, V. Complementary localization and lateralization of orienting and motor attention. *Nat. Neurosci.* **4**, 656–661 (2001).

32. Corbetta, M. *et al.* Common behavioral clusters and subcortical anatomy in stroke. *Neuron* **85**, 927–941 (2015).

33. Fridriksson, J. *et al.* Revealing the dual streams of speech processing. *Proc. Natl. Acad. Sci. U.S.A.* **113**, 15108–15113 (2016).

34. Hartwigsen, G. *et al.* Rapid short-term reorganization in the language network. *Elife* **6**, 1–18 (2017).

35. Sliwinska, M. W., James, A. & Devlin, J. T. Inferior parietal lobule contributions to visual

word recognition. *J. Cogn. Neurosci.* **27**, 593–604 (2015).

36. Hartwigsen, G. *et al.* Short-term modulation of the lesioned language network. *Elife* **9**, (2020).
37. Hartwigsen, G. Flexible Redistribution in Cognitive Networks. *Trends Cogn. Sci.* **22**, 687–698 (2018).
38. Igelström, K. M. & Graziano, M. S. A. The inferior parietal lobule and temporoparietal junction: a network perspective. *Neuropsychologia* **105**, 70–83 (2017).
39. Krall, S. C. *et al.* The right temporoparietal junction in attention and social interaction: a transcranial magnetic stimulation study. *Hum. Brain Mapp.* **37**, 796–807 (2016).
40. Samson, D., Apperly, I. A., Chiavarino, C. & Humphreys, G. W. Left temporoparietal junction is necessary for representing someone else's belief. *Nat. Neurosci.* **7**, 499–500 (2004).
41. Lee, S. M. & McCarthy, G. Functional heterogeneity and convergence in the right temporoparietal junction. *Cereb. Cortex* **26**, 1108–1116 (2016).
42. Tettamanti, M. *et al.* Effective connectivity gateways to the Theory of Mind network in processing communicative intention. *Neuroimage* **155**, 169–176 (2017).
43. Van Overwalle, F., Van de Steen, F., van Dun, K. & Heleven, E. Connectivity between the cerebrum and cerebellum during social and non-social sequencing using dynamic causal modelling. *Neuroimage* **206**, 116326 (2020).
44. Fukuda, H. *et al.* Computing social value conversion in the human brain. *J. Neurosci.* **39**, 5153–5172 (2019).
45. Chambon, V. *et al.* Neural coding of prior expectations in hierarchical intention inference. *Sci. Rep.* **7**, 1278 (2017).
46. Ren, Y. *et al.* Effective connectivity of the anterior hippocampus predicts recollection confidence during natural memory retrieval. *Nat. Commun.* **9**, 4875 (2018).
47. Andrews-Hanna, J. R., Reidler, J. S., Sepulcre, J., Poulin, R. & Buckner, R. L. Functional-anatomic fractionation of the brain's default network. *Neuron* **65**, 550–562 (2010).
48. Schuwerk, T., Schurz, M., Müller, F., Rupprecht, R. & Sommer, M. The rTPJ's overarching

cognitive function in networks for attention and theory of mind. *Soc. Cogn. Affect. Neurosci.* **12**, 157–168 (2017).

49. Mar, R. A. The neural bases of social cognition and story comprehension. *Annu. Rev. Psychol.* **62**, 103–134 (2011).
50. Oldfield, R. C. The assessment and analysis of handedness: the Edinburgh inventory. *Neuropsychologia* **9**, 97–113 (1971).
51. Durnez, J., Blair, R. & Poldrack, R. A. Neurodesign: optimal experimental designs for task fMRI. *bioRxiv* (2018) doi:10.1101/119594.
52. Binder, J. R. *et al.* Neural correlates of lexical access during visual word recognition. *J. Cogn. Neurosci.* **15**, 372–393 (2003).
53. Binder, J. R., Westbury, C. F., McKiernan, K. A., Possing, E. T. & Medler, D. A. Distinct brain systems for processing concrete and abstract concepts. *J. Cogn. Neurosci.* **17**, 905–917 (2005).
54. Brysbaert, M. *et al.* The word frequency effect: a review of recent developments and implications for the choice of frequency estimates in German. *Exp. Psychol.* **58**, 412–424 (2011).
55. Kanske, P. & Kotz, S. A. Cross-modal validation of the Leipzig Affective Norms for German (LANG). *Behav. Res. Methods* **43**, 409–413 (2011).
56. Keuleers, E. & Brysbaert, M. Wuggy: a multilingual pseudoword generator. *Behav. Res. Methods* **42**, 627–633 (2010).
57. Baron-Cohen, S., Leslie, A. M. & Frith, U. Does the autistic child have a 'theory of mind'? *Cognition* **21**, 37–46 (1985).
58. Wimmer, H. & Perner, J. Beliefs about beliefs: representation and constraining function of wrong beliefs in young children's understanding of deception. *Cognition* **13**, 103–128 (1983).
59. Rothmayr, C. *et al.* Common and distinct neural networks for false-belief reasoning and inhibitory control. *Neuroimage* **56**, 1705–1713 (2011).

60. Abdulrahman, H. & Henson, R. N. Effect of trial-to-trial variability on optimal event-related fMRI design: Implications for Beta-series correlation and multi-voxel pattern analysis. *Neuroimage* **125**, 756–766 (2016).

61. Amunts, K. & Zilles, K. Advances in cytoarchitectonic mapping of the human cerebral cortex. *Neuroimaging Clin. N. Am.* **11**, 151–69, vii (2001).

62. Eickhoff, S. B. *et al.* A new SPM toolbox for combining probabilistic cytoarchitectonic maps and functional imaging data. *Neuroimage* **25**, 1325–1335 (2005).

63. Lloyd, S. Least squares quantization in PCM. *IEEE Trans. Inf.* **28**, 129–137 (1982).

64. Eickhoff, S. B., Thirion, B., Varoquaux, G. & Bzdok, D. Connectivity-based parcellation: critique and implications. *Hum. Brain Mapp.* **36**, 4771–4792 (2015).

65. Hartigan, J. A. & Wong, M. A. Algorithm AS 136: A K-Means Clustering Algorithm. *J. Appl. Stat.* **28**, 100 (1979).

66. Thirion, B., Varoquaux, G., Dohmatob, E. & Poline, J.-B. Which fMRI clustering gives good brain parcellations? *Front. Neurosci.* **8**, 167 (2014).

67. Charrad, M., Ghazzali, N., Boiteau, V. & Niknafs, A. NbClust: An R package for determining the relevant number of clusters in a data set. *J. Stat. Softw.* **61**, 1–36 (2014).

68. Abraham, A. *et al.* Machine learning for neuroimaging with scikit-learn. *Front. Neuroinform.* **8**, 14 (2014).

69. Pedregosa, F. *et al.* Scikit-learn: machine Learning in Python. *J. Mach. Learn. Res.* **12**, 2825–2830 (2011).

70. Schaefer, A. *et al.* Local-global parcellation of the human cerebral cortex from intrinsic functional connectivity MRI. *Cereb. Cortex* **28**, 3095–3114 (2018).

71. Karrer, T. M. *et al.* Brain-based ranking of cognitive domains to predict schizophrenia. *Hum. Brain Mapp.* **40**, 4487–4507 (2019).

72. Friston, K., Moran, R. & Seth, A. K. Analysing connectivity with Granger causality and dynamic causal modelling. *Curr. Opin. Neurobiol.* **23**, 172–178 (2013).

73. Zeidman, P. *et al.* A guide to group effective connectivity analysis, part 1: First level analysis with DCM for fMRI. *Neuroimage* **200**, 174–190 (2019).

74. Seghier, M. L. & Friston, K. J. Network discovery with large DCMs. *Neuroimage* **68**, 181–191 (2013).

75. Friston, K. & Penny, W. Post hoc Bayesian model selection. *Neuroimage* **56**, 2089–2099 (2011).

76. Rosa, M. J., Friston, K. & Penny, W. Post-hoc selection of dynamic causal models. *J. Neurosci. Methods* **208**, 66–78 (2012).

77. Stephan, K. E., Penny, W. D., Daunizeau, J., Moran, R. J. & Friston, K. J. Bayesian Model Selection for Group Studies. *NeuroImage* **47**, 1004–1017 (2009).

78. Ahrens, J., Geveci, B. & Law, C. ParaView: an end-user tool for large-data visualization. in *The Visualization Handbook* (ed. Hansen, C.D. & Johnson, C.R.) 717–731 (2005).

79. Gu, Z., Gu, L., Eils, R., Schlesner, M. & Brors, B. circlize implements and enhances circular visualization in R. *Bioinformatics* **30**, 2811–2812 (2014).

80. Xia, M., Wang, J. & He, Y. BrainNet Viewer: a network visualization tool for human brain connectomics. *PLoS One* **8**, e68910 (2013).

81. Mazziotta, J. *et al.* A probabilistic atlas and reference system for the human brain: International Consortium for Brain Mapping (ICBM). *Philos. Trans. R. Soc. Lond. B Biol. Sci.* **356**, 1293–1322 (2001).

82. Fischl, B., Sereno, M. I., Tootell, R. B. H. & Dale, A. M. High-resolution intersubject averaging and a coordinate system for the cortical surface. *Hum. Brain Mapp.* **8**, 272–284 (1999).

83. Wu, J. *et al.* Accurate nonlinear mapping between MNI volumetric and FreeSurfer surface coordinate systems. *Hum. Brain Mapp.* **39**, 3793–3808 (2018).